

# Tunable rectangular array illuminator in periodically poled LiNbO<sub>3</sub> crystal

Qiuying Li (李秋颖), Juan Huo (霍娟), Xiaohui Zhao (赵晓晖), and Xianfeng Chen (陈险峰)\*

State Key Laboratory on Fiber Optic Local Area Communication Networks and Advanced Optical Communication Systems,  
Department of Physics, Shanghai Jiao Tong University, Shanghai 200240, China

\*Corresponding author: xfchen@sjtu.edu.cn

Received December 29, 2013; accepted March 27, 2014; posted online April 30, 2014

An electro-optic tunable rectangular array illuminator in one-dimensional periodically poled LiNbO<sub>3</sub> (PPLN) crystal is presented experimentally which result is in good agreement with results from simulation. The illuminator is formed based on the Talbot self-imaging effect by applying an electric field on PPLN. The intensity distribution of rectangular array could be precisely modulated. Compared with other array illuminators, this tunable illuminator uses a lower voltage and could get a more concentrated intensity distribution. The influence of the incident angle to the self-imaging patterns is studied for the first time.

OCIS codes: 070.6760, 160.2100.  
doi: 10.3788/COL201412.050701.

Array illuminator is a device that transforms laser beam into patterns with periodical optical intensity and is widely used in processing and synthesis, photolithography, optical testing, optical metrology, spectrometry, optical computing, as well as in electron optics and microscopy<sup>[1–3]</sup>. Although several schemes have been proposed for implementing array illuminators, the favorite method is Talbot effect. It is a near-field diffraction phenomenon in which self-imaging of a grating or other periodic structure replicates at certain imaging planes, was found by Talbot *et al.*<sup>[4–6]</sup>.

In this letter, we realized a rectangular array illuminator that was made by a phase grating which was a one-dimensional (1D) periodically poled LiNbO<sub>3</sub> (PPLN) with an external electric field. The PPLN was formed through ferroelectric domain inversion technology<sup>[7]</sup>, the nonlinear optical coefficient and the electro-optic (EO) coefficient are modulated periodically. Based on this structure, essential applications such as quasi-phase-matching<sup>[8]</sup>, wavelength conversion<sup>[9]</sup>, narrow band solc-type filters<sup>[10,11]</sup>, polarization controllers<sup>[12,13]</sup>, optical vortex<sup>[14]</sup>, all-optical logic gates<sup>[15]</sup>, waveguide<sup>[16]</sup> and laser Q-switch<sup>[17]</sup> have been successfully demonstrated. Compared with other electro-optic phase illuminators<sup>[18,19]</sup>, there are some important features of our device. In our experiment the light was chosen to propagate parallel to the  $y$  axis and the direction of polarization was along the  $z$  axis. These specific arrangements increased the phase delay between positive domains and negative domains, consequently, the relevant modulating voltage became lower. The increased external electric field will induce the decrease in width of bright areas in the self-imaging patterns, method to acquire more concentrated distribution of intensity was proposed. We studied the self-imaging patterns at different incident angles. Some interesting patterns were recorded, such as the chirp intensity distribution.

Benefitting from the modulation of EO coefficient and the reversal of the ferroelectric, the phase changes periodically on the output surface after applying an electric field along the  $z$  axis of PPLN. A rectangular phase

grating with periodic structures is formed. As mentioned before, the Talbot effect can be found attributed to the interference of diffracted beams from periodic structures. In the experiment, as mentioned before, the light propagated along the  $y$  axis and the direction of polarization paralleled to the  $z$  axis (extraordinary light). The change of refractive index and phase in domains can be written as<sup>[20]</sup>,

$$\Delta n = \pm \frac{1}{2} n_e^3 \gamma_{33} E_z, \quad (1)$$

$$\Delta \phi = \frac{l_y \Delta n}{2\pi \lambda}, \quad (2)$$

where  $n_e$  is refractive index of extraordinary light without electric field,  $\gamma_{33}$  is linear electro-optic coefficient of the lithium niobate crystal,  $l_y$  is the length along the  $y$  direction of PPLN, and  $E_z$  is the electric field strength applied on the  $z$  direction. In PPLN,  $\gamma_{33}$  is nearly three times as large as  $\gamma_{13}$ , and the latter will appear when the ordinary light is chosen as Eq. (1) turns to be  $\Delta n = \pm 1/2 n_o^3 \gamma_{13} E_z$ . And because of limit of domain inversion technology, the length of PPLN along the  $z$  axis is short, the maximum is 1 mm in general, however the length along the  $y$  direction could be manufactured to be considerably long. Here we chose  $l_y = 3$  mm. Consequently, compared with other electro-optic phase illuminators, our case could use an extremely low electric field to get a prospective phase delay.

The transmittance function of this phase grating is given by

$$t(x, y) = \left[ (e^{i\Delta\phi} - e^{-i\Delta\phi}) \text{rect} \left( \frac{2x}{a} \right) \right] * \frac{1}{a} \text{comb} \left( \frac{x}{a} \right) + e^{i\Delta\phi}, \quad (3)$$

where  $*$  represents convolution and  $a$  is the period of grating. The transfer function of Fresnel diffraction can be written as

$$h(x, y) = \frac{\exp(ikz)}{i\lambda z} \exp \left[ \frac{ik}{2z} (x^2 + y^2) \right], \quad (4)$$

and the distribution of diffraction intensity at  $z$  position from the output plane of PPLN can be deduced from the Fresnel diffraction formula as

$$U(x, y) = t(x, y) * h(x, y), \quad (5)$$

The experiment setup is shown in Fig.1. The PPLN we chose in our experiment was fabricated via standard electric field poling of a Z-cut LiNbO<sub>3</sub> crystal at room temperature 25 °C<sup>[7]</sup>. The dimension of the poled crystal was  $15(x) \times 3(y) \times 1(z)$  (mm), with the inversion periods of 19.43  $\mu\text{m}$  (duty ratio of 1:1). The optical axis of PPLN crystal was parallel to the  $z$  axis. He-Ne Laser was used to produce input beam at 632.8 nm. The laser propagated along the  $y$  axis of the PPLN crystals and firstly passed through the polarizer to make the polarization of light along the  $z$  axis, and was then reshaped by a telescope device, composed of two focusing lenses, to achieve a near-parallel beam with a spot size of 100  $\mu\text{m}$ . After external electric field being applied along the  $z$  axis a phase grating was generated in the crystal. We used a 40 $\times$  objective lens to magnify the self-imaging patterns and the output light was projected onto a charge-coupled device (CCD) camera. By adjusting the position of the objective lens, which was controlled by a precision translation stage, the intensity pattern at different imaging planes could be recorded. Because the Talbot effect was a lensless self-imaging, the objective lens and the CCD camera were only used for easy observations. The Talbot distance is calculated to be  $z_t = 2a^2/\lambda = 1192 \mu\text{m}$ , where  $a = 19.43 \mu\text{m}$  is the inversion period of PPLN crystal.

In the experiment, the self-imaging patterns were firstly recorded at the electric field  $E = 1.7 \text{ kV/mm}$ . The first picture, recorded by optical microscope, displays the structure of domain of PPLN in the incidence direction (Fig. 2(a)). Figure 2(f) shows the intensity distribution at the output plane of PPLN. In fact, the phases in positive domain and negative domain experience same change in absolute value, this kind of phase change cannot have an effect on intensity distribution. Actually, the domain walls<sup>[21]</sup> in PPLN is a kind of special structure whose refractive index is different from domains, the presence of domain walls leads to the appearance of dark rectangular stripes as shown in Fig. 2(f). As the distance increases, the bright rectangular stripes become slender which means the intensity is more and more concentrated. When  $z = 1/4z_t$ , the bright stripes are the finest (Figs. 2(b), (g)). The simulation is in good with experiment. The period of these light stripes is the same with PPLN, 19.43  $\mu\text{m}$ . Through this method we get an easy way to acquire laser stripe with intensity periodicity. We then increased the distance to  $z = 1/2z_t$ . The recorded pattern (Figs. 2(c) and (h)) becomes similar to Fig. 2(f). However, there is one obvious difference between Figs. 2(h) and (f). In Fig. 2(h), there is a black spot which is owing to the imperfections in the surface

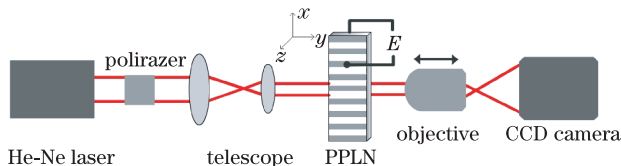


Fig. 1. Experimental setup.

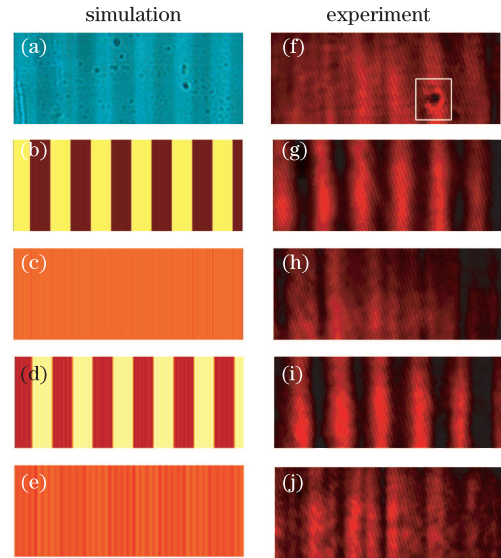


Fig. 2. Recorded self-imaging patterns at different Talbot lengths. Left column, simulation, right column: experiment. (a) The structure of domain along the  $y$  direction of PPLN recorded by Olympus BX51 microscope; (f) Intensity distribution at the output plane of PPLN; (b, g) Recorded patterns at  $z = 1/4z_t$ ; (c, h) Recorded patterns at  $z = 1/2z_t$ ; (d, i) Recorded patterns at  $z = 3/4z_t$ ; (e, j) Recorded patterns at  $z = z_t$ .

(the marked square), while the self-imaging (Fig. 2(h)) produces an uniform interference pattern, which is attributed to the Talbot effect that only the periodically distributed light is self-imaged at half Talbot plane. This could be useful for the application of optical lithography. Figure 2(c) demonstrates a homogeneous intensity distribution in the simulation, this kind of distribution is attributed to the quasi self-imaging of the grating (the difference of phase between here and the output plane is  $\pi$ ), therefore, because of the special phase grating, this distribution should be the same as that at the output plane of PPLN. As mentioned before, the domain walls will lead to the appearance of dark rectangular stripes in Fig. 2(f), this makes the minor differences with Fig. 2(c). When  $z = 3/4z_t$ , the rectangular stripe structure appears again (Figs. 2(d) and (i)). But a difference emerges compared with the pattern at  $z = 1/4z_t$ , the position of bright areas and dark areas have exchanged. That means the difference of phase between  $z = 1/4z_t$  and  $z = 3/4z_t$  is  $\pi$ . This exchange phenomenon could have potential application in optical encryption. When the observer plane is at the first Talbot distance (Figs. 2(e) and (j)),  $z = z_t$ , the pattern becomes similar to Fig. 2(f) again, it has the same phase and intensity distribution with output plane, so it is the real self-imaging of the phase grating (Although Fig. 2(h) is the same to Fig. 2(f), the phase between Fig. 2(h) and (f) is  $\pi$ ). Above phenomena will arise periodically as the position of observe plane moving continuously. However, when the distance became fairly large the stripes became obscure.

The influence on the intensity distribution of the electric field was also studied. We fixed the distance at  $z = 1/5z_t = 250 \mu\text{m}$ , and changed the electric field. Four pictures has been recorded at  $E = 0.1 \text{ kV/mm}$ ,  $E = 0.6$

kV/mm,  $E = 1.2$  kV/mm,  $E = 1.8$  kV/mm, respectively (Figs. 3(a-h)). The simulation results are well agreeable with experiment. It is easy to discover that these bright stripes become more and more slender with the increase of the electric field. Different from changing the distance, the middle position of the bright and dark stripes is invariable. This means that intensity is concentrated to the middle of the bright stripes gradually. The higher electric field produces the larger difference between the phases of the positive domains and negative domains in the PPLN, although the change of refractive index here is fairly small, the order of magnitudes is  $10^{-4}$ , the impact to the intensity distribution is rather huge. In our experiment, the highest electric field is 1.8 kV/mm, further enhancing the voltage could lead breakdown of air in our experiment. The simulation has proved that when the electric field is fairly high, about 2.3 kV/mm, the change of refractive index is almost  $10^{-3}$ , the intensity of the laser will concentrate on an area with the width  $1 \mu\text{m}$ . And after the electric field increases, the period of the image will reduce to half. This could provide a method to acquire quite concentrated distribution of light intensity and the self-imaging with manifold period if we use the material whose phase is much more sensitive to the applying electric field.

We also recorded patterns at two special incident angles. We found that the intensity distribution at some Talbot planes is not only sensitive to the distance and electric field, but also the incident angle. The first picture (Figs. 4(a,c)) recorded at  $1^\circ$ ,  $E = 1$  kV/mm and  $z = 0.3z_t$  shows that every bright stripe divides into two, that means the period of intensity distribution is reduced by half. When the incident angle becomes  $2.5^\circ$ , and  $E = 1.61$  kV/mm at  $z = 1/2z_t$ , a chirp intensity distribution appears, the width of bright strips decreases progressively (Figs. 4(b,d)). It could be explained as the following. The existence of incident angle leads the distance between PPLN output plane and observer plane to increase progressively, as mentioned before the width of bright strips changes with the distance, so the different width could appear. This sensitivity to the incident angle

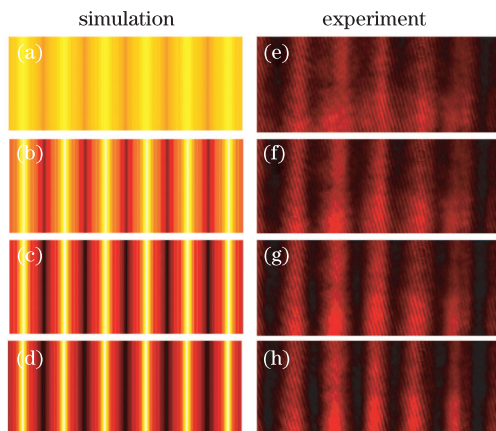


Fig. 3. Recorded self-imaging patterns at  $z = 1/5z_t$  and different electric field. Left column: simulation, right column: experiment. (a, e) Recorded patterns at  $E = 0.1$  kV/mm; (b, f) Recorded patterns at  $E = 0.6$  kV/mm; (c, g) Recorded patterns at  $E = 1.2$  kV/mm; (d, h) Recorded patterns at  $E = 1.8$  kV/mm.

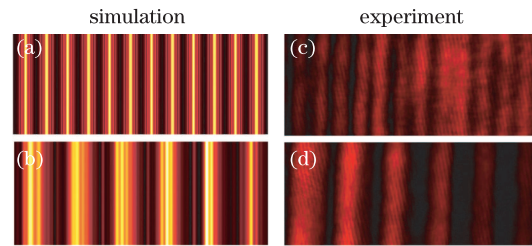


Fig. 4. Patterns at two special angles of incidence. Left column: simulation, right column: experiment. (a,c) The period is reduced by half at  $1^\circ$ ,  $E = 1$  kV/mm and  $z = 0.3z_t$ ; (b,d) Chirp intensity distribution at  $2.5^\circ$ ,  $E = 1.61$  kV/mm and  $z = 1/2z_t$ .

could make the Talbot self-imaging have more potential applications in the future. We also found this angle related Talbot effect is susceptible to the length along the light propagation. When the length becomes short, about 1 mm, this angle influence to the self-imaging patterns weakens.

In conclusion, we investigate the tunable rectangular array illuminator in PPLN crystal by applying an electric field at integer and fractional Talbot distance. We find that the intensity distribution is much sensitive to the precision position of observer plane and the applied electric field, even to the angle of incidence. We realized a kind of rectangular phase array illuminator with a relatively low voltage and studied the self-imaging patterns at different incident angle for the first time. This flexibly tunable Talbot self-imaging can display varied intensity distribution patterns and may make Talbot effect more useful in optical technologies.

This work was supported by the National Basic Research Program of China (No. 2011CB808101), the National Natural Science Foundation of China (No. 61125503 and 61235009) and the Foundation for Development of Science and Technology of Shanghai (No. 1313JC1408300).

## References

1. V. Arrizon and J. Ojeda-Castaneda, *Opt. Lett.* **20**, 180 (1995).
2. P. Xi, C. Zhou, E. Dai, and L. Liu, *Opt. Lett.* **27**, 228 (2002).
3. C. S. Guo, X. Yin, L. W. Zhu, and Z. P. Hong, *Opt. Lett.* **32**, 2079 (2007).
4. H. F. Talbot, *Philosophical Magazine Series 3* **9**, 401 (1836).
5. L. Rayleigh, *Philosophical Magazine Series 5* **11**, 196 (1881).
6. J. Wen, Y. Zhang, and M. Xiao, *Adv. Opt. Photon.* **5**, 83 (2013).
7. M. Yamada, N. Nada, M. Saitoh, and K. Watanabe, *Appl. Phys. Lett.* **62**, 435 (1993).
8. X. Hu, P. Xu, and S. Zhu, *Photon. Res.* **1**, 171 (2013).
9. C. Q. Xu, H. Okayama, and M. Kawahara, *Appl. Phys. Lett.* (1993).
10. X. Chen, J. Shi, Y. Chen, Y. Zhu, Y. Xia, and Y. Chen, *Opt. Lett.* **28**, 2115 (2003).
11. Y. Chen and Y. Huang, *Opt. Lett.* **28**, 1460 (2003).
12. K. Liu and X. Chen, *Phys. Rev. A* **80**, 063808 (2009).

13. K. Liu, J. Shi, and X. Chen, *Opt. Lett.* **34**, 1051 (2009).
14. L. S. Lei Shi, L. T. Linghao Tian, and X. C. Xianfeng Chen, *Chin. Opt. Lett.* **10**, 0501 (2012).
15. Y. Tang, Y. Chen, H. Jiang, W. Ji, Y. Wu, and X. Chen, *Chin. Opt. Lett.* **11**, 061901 (2013).
16. L. Ye, J. Wang, H. Hu, J. Yu, and K. Song, *Chin. Opt. Lett.* **11**, 110604 (2013).
17. K. Liu, J. Shi, and X. Chen, *Appl. Phys. Lett.* **94**, 101106 (2009).
18. M. Paturzo, P. De Natale, S. De Nicola, P. Ferraro, S. Mailis, R. Eason, G. Coppola, M. Iodice, and M. Gioffré, *Opt. Lett.* **31**, 3164 (2006).
19. J. Zhang and Y. Chen, *Quantum Electronics* **49**, 471 (2013).
20. Y.-Q. Lu, Z.-L. Wan, Q. Wang, Y.-X. Xi, and N.-B. Ming, *Appl. Phys. Lett.* **77**, 3719 (2000).
21. T. Yang, V. Gopalan, P. Swart, and U. Mohideen, *Phys. Rev. Lett.* **82**, 4106 (1999).